# Effect of Higher Order Modes in Standard Spherical Near-Field Probe Correction

A.C. Newell, S.F. Gregson
Nearfield Systems Inc.
19730 Magellan Drive,
Torrance, CA 90502-1104
anewell@nearfield.com, sgregson@nearfield.com

***Abstract*— Within the standard scheme for probe-corrected spherical data-processing, it has been found that for an efficient computational implementation it is necessary to restrict the characteristics of the probe pattern such that it contains only azimuthal modes for which μ = ±1 [1, 2, 3]. This first-order pattern restriction does not however extend to placing a limit on the polar index mode content and therefore leaves the directivity of the probe unconstrained. Clearly, when using this widely utilized approach, errors will be present within the calculated probe-corrected test antenna spherical mode coefficients for cases where the probe is considered to have purely modes for which μ = ±1 and where the probe actually exhibits higher order mode structure. A number of analysis [4, 5, 6, 7, 8] and simulations [9, 10, 11, 12] can be found documented within the open literature that estimate the effect of using a probe with higher order modes. The following study is a further attempt to develop guidelines for the azimuthal and polar properties of the probe pattern and the measurement configuration that can be utilized to reduce the effect of higher order spherical modes to acceptable levels. Included in this study are the cases when an Open Ended Waveguide (OEWG) is simulated at a series of measurement distances, a Quad Ridged Horn Probe (QRHP) with very large higher order modes is also simulated, the AUT is offset from the origin of the measurement sphere and the AUT is simulated with its main beam along the equator rather than along the pole. These new simulation cases provide additional guidelines when selecting a probe for spherical near-field measurements and answer some questions that have been raised about generalizing past results.**

**Index Terms*— near-field, measurements, near-field probe, spherical, spherical mode analysis, probe pattern, higher order probes, equatorial mode.***

## I INTRODUCTION

The details of the existing simulation algorithm have been described in detail in previous publications [9, 10, 11, 12] and will merely be summarized here with the necessary modification to enable the simulation of equatorial mode spherical near-field data being highlighted. The simulation begins by using previously measured spherical near-field data for both the antenna under test (AUT) and a scanning probe to calculate the far-field patterns of both antennas over a full far-field sphere. The AUT far-field pattern is then rotated mathematically about the *z*-axis to simulate a ϕ-rotation and about the *y*-axis to simulate a θ-rotation. The transmitting plane wave spectrum over the forward hemisphere on a *k*-space, $(k_x, k_y)$ grid is then derived for each of the rotated AUT patterns. These plane-wave spectra represent the AUT rotated in ϕ and θ exactly as it is in a spherical near-field measurement. Whilst this approach is effective for simulating polar mode spherical near-field measurements, a different approach is needed when simulating equatorial measurements where the boresight direction of AUT is assumed to nominally point in the θ = 90° equatorial region. Thus, an additional step is required in the simulation software to implement this change in the antenna-to-range alignment. A number of strategies could be adopted however perhaps the simplest is to recognize that the elevation over azimuth (α,ε) co-ordinate system corresponds to a conventional spherical system when used in equatorial mode [13]. Thus, by specifying the required (θ,ϕ) pattern angles and by mapping these to the corresponding (α,ε) angles, *i.e.* α = θ - 90°, ε = ϕ, the AUT far-field pattern is then rotated mathematically about the *y*-axis to simulate an α-rotation and then about the *x*-axis to simulate an ε-rotation where the rotations are applied sequentially in that order. This insures that the directions and unit vectors are correctly preserved. Although it is possible to use a far-field antenna pattern from an actual equatorial mode measurement as the basis for the simulation, this technique has the inherent advantage that when comparing results with the existing polar-mode simulations the same AUT patterns can be used with either software with no external additional changes being required. The remainder of the processing is in common with the polar-mode simulation. Thus, as before, the far-field probe pattern is rotated about its *z*-axis to simulate the χ-rotations of 0° and 90° and its receiving plane wave spectrum calculated on the same *k*-space grid as the AUT. The calculation of a receiving plane-wave spectrum for the two χ rotations of the open ended waveguide (OEWG) probe is repeated but in this case, the spherical modes for $\mu \neq \pm 1$ are set to zero in the calculation of its far-field pattern. The two spectra represent respectively a higher order probe and a first order probe with

otherwise identical patterns and polarization. For the remaining steps in the simulation a computer program was developed to use the rotated plane-wave spectra of the AUT and one of the probes to calculate the output of the probe for a specified $x$, $y$, $z$ position of the probe. When $x = y = 0$, the probe is at the equator of the measurement sphere and the AUT is positioned at the origin of the sphere or along the $x$-axis. Offset positions of the AUT can be simulated by selecting non-zero values for $x$, $y$ or $z$ when calculating the AUT far-field pattern. The $z$-position of the probe defines the measurement radius. The probe output is produced using the planar near-field transmission equation,

$$b'_0(x,y,z,\theta,\phi,\chi) = F' a_0 \int\int \underline{t}_{10}(\underline{K},\theta,\phi)\cdot \underline{s}'_{02}(\underline{K},\chi) e^{iyz} e^{i(k_x x + k_y y)} dk_x dk_y \quad (1)$$

Here, $a_0$ is the input amplitude and phase to the AUT, $b'_0(x,y,z,\theta,\phi,\chi)$ is the probe output amplitude and phase for the probe at $(x,y,z)$ and rotated about the probe z-axis by the angle $\chi$ AUT rotated by $\theta$ and $\phi$, $\underline{t}'_{10}(\underline{K},\theta,\phi)$ is the AUT plane-wave transmitting spectrum rotated by $\theta$ and $\phi$, $\underline{s}'_{02}(\underline{K},\chi)$ is the probe plane-wave receiving spectrum for $\chi$ rotation. The rotation angles $\theta$, $\phi$, *and* $\chi$ have been added as variables to the probe output, the AUT spectrum and the probe receiving spectrum to show that the planar transmission equation will be used to produce simulated spherical near-field data at arbitrary $\theta$ *and* $\phi$ positions on the measurement sphere with arbitrary $\chi$ rotations of the probe. The planar transmission equation is used for the simulation rather than the spherical transmission equation since both are equally valid and accurate expressions for the transmission between a test antenna and a probe at any arbitrary near-field position and relative orientation. The planar equation is much easier to calculate numerically and can be used *without* modification for both first-order *and* higher-order probes.

## II Simulation Details

The AUT for most of the simulations was a high gain x-band slotted waveguide array and its far-field pattern is shown in Figure 1. A Standard Gain Horn (SGH) was also simulated as the AUT to produce more general results. Two different AUT orientations were also simulated for even more generalization. In the polar orientation, the AUT is mounted with its main beam along or near to the Z-axis of the reference coordinate system. The measured $\theta$ and $\phi$ components have nearly equal peak amplitudes and both components must be acquired to produce the main and cross component far-field patterns. In the equatorial orientation, the AUT is mounted with its main beam normal to the Z-axis and for linearly polarized antennas, one near-field component may be very small. This orientation is often used for fan beam antennas. To generalize the simulation as far as possible, the simulated measurement radios was specified as a multiple of the maximum radial extent (MRE) of the AUT thereby allowing generalization of the results to other probe/AUT combinations. In this case the AUT had a conceptual MRE of 18" (0.46 m).

The first series of simulations used the $TE_{10}$ fed rectangular OEWG as the probe at a number of measurement radii. The amplitudes of the probe's spherical modes for $s = 1$ are shown in Figure 2 and the largest amplitude for the higher order modes occurs at $m = 3$ and is only 20 dB below the First Order (FO) mode for $m = 1$.

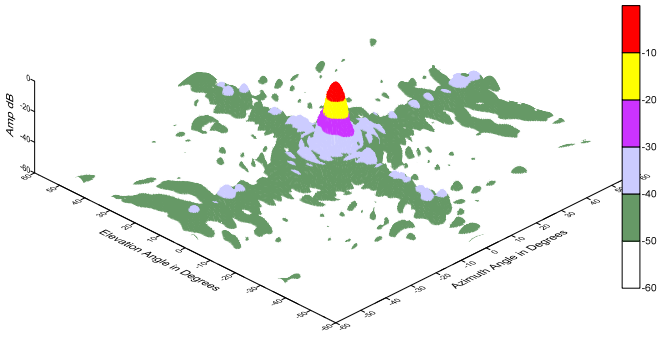


Figure 1 Main component far-field pattern of AUT used in the simulation.

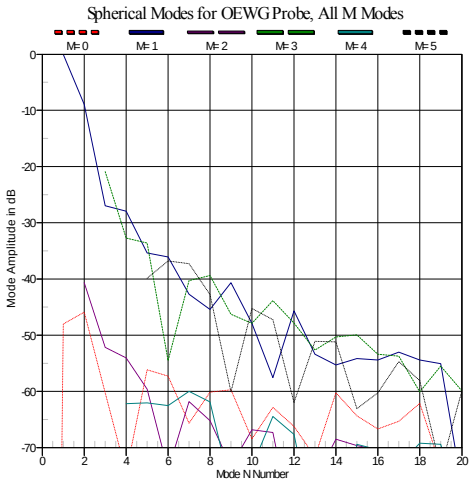


Figure 2 Spherical mode amplitudes for rectangular OEWG probe.

Simulations were produced for the AUT in the polar orientation with the OEWG probe using all its modes and only the FO modes and the spherical near-field and far-field patterns were computed using the standard spherical software that uses only the FO modes in the probe correction. As a check on the complete process, the simulated AUT far-field pattern using all the probe modes was compared to the AUT far-field that was used as the input to the simulation program. The difference between these patterns is an indication of the effect of approximations used in the rotation and interpolation of the simulation process. Figure 3 shows one example of this comparison and the RMS ERR/SIG level of -54 dB verifies

that it is very accurate. This difference does not indicate the lower limit of the simulations ability to detect the effect of the higher order modes in the probe correction process. Both of the far-field patterns compared in that process are produced from simulated data and have the same approximations due to numerical processing which cancel out when compared. The following results will illustrate that reliable higher order mode effects at levels of -80 to -90 dB below the peak far-field are possible.

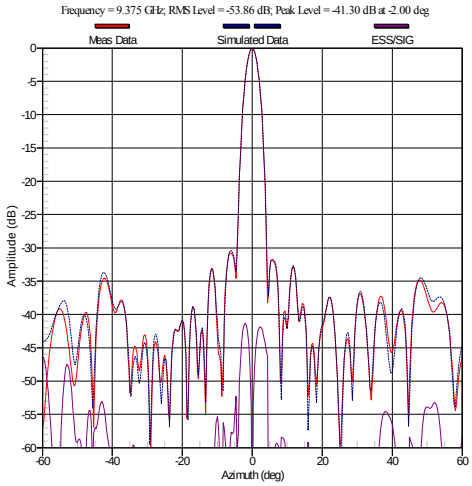


Figure 3 Comparison between far-field patterns computed from measured and simulated data.

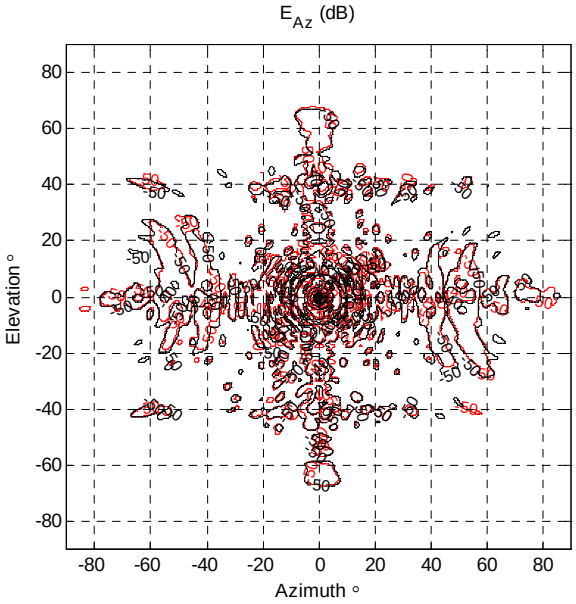


Figure 4 Input AUT far-field pattern and simulated pattern for the equatorial orientation showing excellent agreement down below -60 dB.

A more extensive comparison between the input AUT far-field and the simulated pattern is shown in Figure 4 for the case where the AUT was simulated in the equatorial orientation. This simulation required a new, additional process to rotate the AUT pattern from the polar to the equatorial orientation. The agreement is evidence of the validity of the new step and the overall simulation process.

Simulations with differences between the higher order and FO OEWG probe were produced for measurement distances of 1, 2, 3 and 4 MRE and the difference graphs are shown for the minimum and maximum distances in Figures 5 and 6.

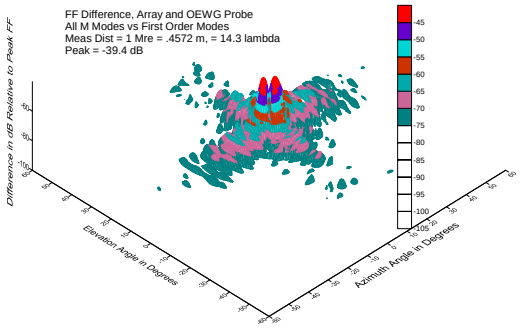


Figure 5 Far Field difference, OEWG probe, Z = 1 * MRE

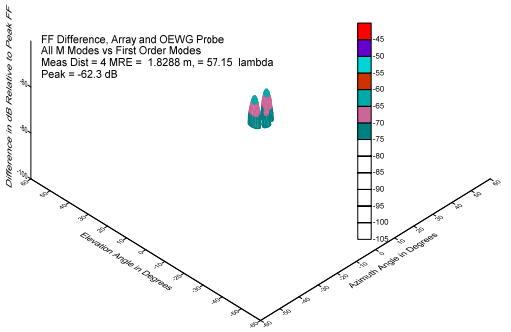


Figure 6 Far field difference, OEWG Z = 4*MRE

Simulations were also carried out using a quad ridged horn probe that is representative of a broad band probe that might be used to increase the measurement speed by switching between the two polarizations and allowing measurements over multiple bands. These probes can improve the measurement speed, but their higher order modes are also larger than the OEWG. It is desirable to quantify the errors caused by these higher order modes and steps that can be taken to minimalize them. The E and H-Plane patterns for the probe and the spherical mode amplitudes are shown in Figures 7 and 8.

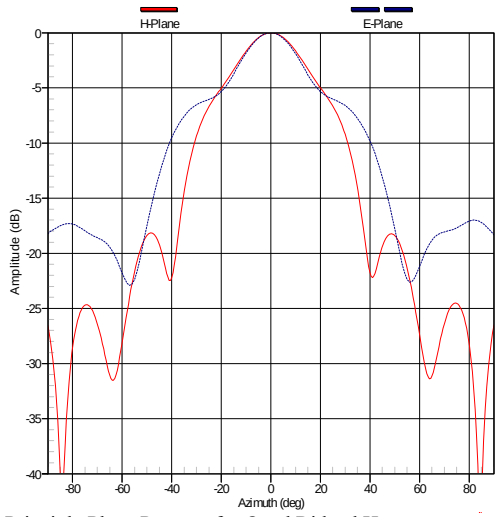


Figure 7 Principle Plane Patterns for Quad Ridged Horn.

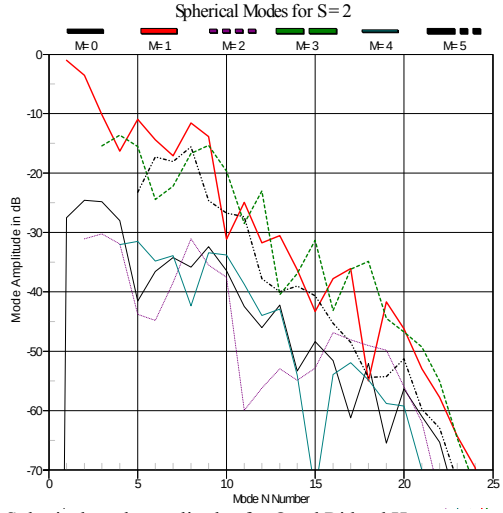


Figure 8 Spherical mode amplitudes for Quad Ridged Horn.

The far-field error/far-field peak graphics similar to Figures 5 and 6 were produced for the horn probe and they had the same general character as the OEWG probe results. The error peak and the angular region where the error signal was greater than -65 dB were slightly larger. These features are summarized and compared to the OEWG results in Figures 9 and 10 where the peak far-field error and directivity error are plotted as a function of the simulated measurement radius.

Simulations were also performed for the AUT offset from the center of the measurement sphere and for the AUT in the equatorial orientation and these results will be covered in more detail in the presentation. These show that the effect of the higher order modes is not significantly increased by these different antenna configurations.

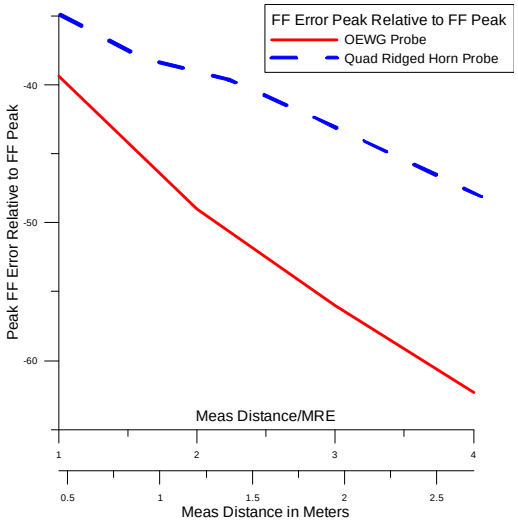


Figure 9 Far-Field error peak due to higher order modes for slotted array AUT.

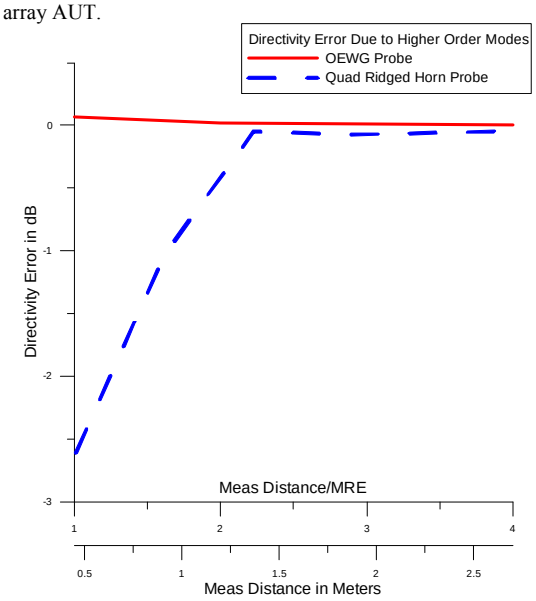


Figure 10 Directivity error due to higher order modes for slotted array AUT.

In near-field measurements where gain of the AUT is required, a pyramidal horn gain standard is often used as the reference and spherical measurements are also performed on the gain standard. This arrangement was also simulated by using the far-field pattern of the gain standard in place of the slotted array. These results are summarized in Figures 11 and 12.

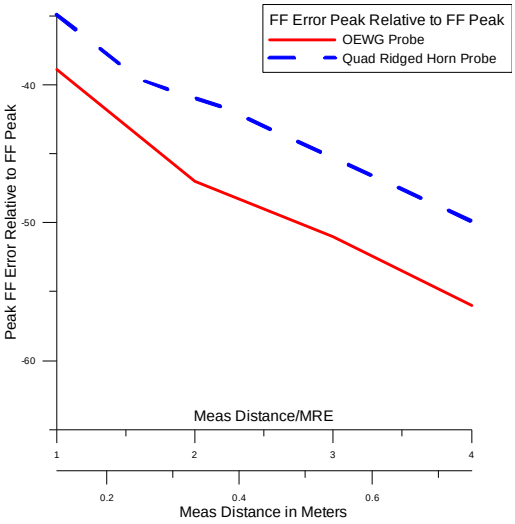


Figure 11 Far-field error peak for standard gain horn with OEWG and quad ridged horn probes.

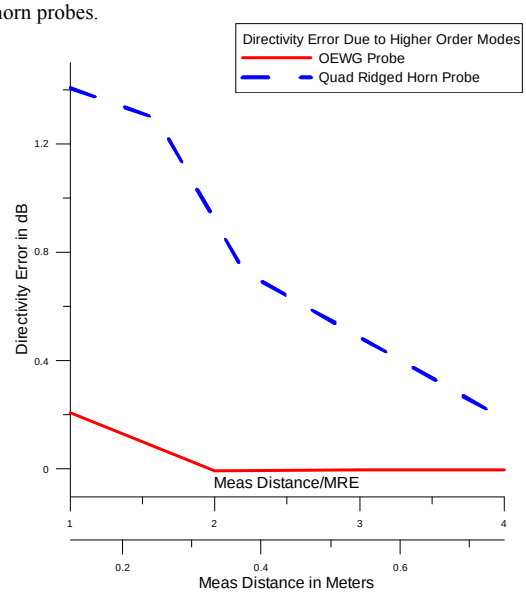


Figure 12 Directivity error for standard gain horn with OEWG and quad ridged horn probes.

The higher order modes of the quad ridged horn do produce significant errors at radii close to the MRE of the SGH, however by increasing the measurement distance sufficiently, the effect can be reduced to acceptable levels.

## III Summary And Conclusions

A powerful, efficient and reliable simulation process has been further developed and demonstrated for a variety of typical spherical near-field measurement configurations. This simulation tool can be used to predict the effect of higher order modes for any proposed or completed combination of AUT, probe AUT orientation and measurement radius. The error in the far-field results due to the higher order modes of the probe can be determined and used to select a probe to improve measurement efficiency and reduce the cost and complexity of the probe while increasing its bandwidth.

The simulations have also confirmed and extended the previous simulation results. When using an OEWG probe, the effect of the higher order modes is limited to the main beam region of the AUT and even at the minimum measurement radius, the error signal level is near -40 dB and can be reduced to below -50 dB by using moderate measurement distances. Other measurement errors will typically be larger. The same error levels can be achieved with a broad band probe by using the simulation to determine the required measurement distance.

## References

[1] P.F. Wacker, "Near-field antenna measurements using a spherical scan: Efficient data reduction with probe correction", Conf. on Precision Electromagnetic Measurements, IEE Conf. Publ. No. 113, pp. 286-288, London, UK, 1974.

[2] F. Jensen, "On the probe compensation for near-field measurements on a sphere", Archiv für Elektronik und Übertragung-stechnik, Vol. 29, No. 7/8, pp. 305-308, 1975.

[3] J.E. Hansen, (Ed.) "Spherical near-field antenna measurements", Peter Peregrinus, Ltd., on behalf of IEE, London, 1988.

[4] T.A. Laitinen, S. Pivnenko, O. Breinbjerg, "Odd-order probe correction technique for spherical near-field antenna measurements," Radio Sci., vol. 40, no. 5, 2005.

[5] T.A. Laitinen, O. Breinbjerg, "A first/third-order probe correction technique for spherical near-field antenna measurements using three probe orientations," IEEE Trans. Antennas Propag., vol. 56, pp. 1259–1268, May 2008.

[6] T.A. Laitinen, J. M. Nielsen, S. Pivnenko, O. Breinbjerg, "On the application range of general high-order probe correction technique in spherical near-field antenna measurements," presented at the 2nd Eur. Conf. on Antennas and Propagation (EuCAP'07), Edinburgh, U.K. Nov. 2007.

[7] T.A. Laitinen, S. Pivnenko, O. Breinbjerg, "Theory and practice of the FFT/matrix inversion technique for probe-corrected spherical near-field antenna measurements with high-order probes", IEEE Trans. Antennas Propag., vol. 58,, No. 8, pp. 2623–2631, August 2010.

[8] T.A. Laitinen, S. Pivnenko, "On the truncation of the azimuthal mode spectrum of high-order probes in probe-corrected spherical near-field antenna measurements" AMTA, Denver, November 2012.

[9] A.C. Newell, S.F. Gregson, "Estimating the effect of higher order modes in spherical near-field probe correction", AMTA 34th Annual Meeting & Symposium, Seattle, WA, October. 2012.

[10] A.C. Newell, S.F. Gregson, "Higher Order Mode probes in Spherical Near-Field Measurements", EuCAP, Gothenburg, April, 2013.

[11] A.C. Newell, S.F. Gregson, "Estimating the Effect of Higher Order Modes in Spherical Near-Field Probe Correction", AMTA 35th Annual Meeting & Symposium, Seattle, WA, October. 2013.

[12] A.C. Newell, S.F. Gregson, "Estimating the Effect of Higher Order Azimuthal Modes in Spherical Near-Field Probe Correction", EuCAP, The Hague, April, 2014.

[13] C.G. Parini, S.F. Gregson, J. McCormick, D. Janse van Rensburg "Theory and Practice of Modern Antenna Range Measurements", IET Press, 2014, ISBN 978-1-84919-560-7.